Proximal tubule H-ferritin mediates iron trafficking in acute kidney injury

Abolfazl Zarjou,[1] Subhashini Bolisetty,[1] Reny Joseph,[1] Amie Traylor,[1] Eugene O. Apostolov,[2] Paolo Arosio,[3] Jozsef Balla,[4] Jill Verlander,[5] Deepak Darshan,[6] Lukas C. Kuhn,[7] and Anupam Agarwal[1,8]

[1]Nephrology Research and Training Center, Division of Nephrology, Department of Medicine, University of Alabama at Birmingham, Birmingham, Alabama, USA. [2]Department of Pharmacology and Toxicology, Department of Internal Medicine, Nephrology, University of Arkansas for Medical Science, Little Rock, Arkansas, USA. [3]Dipartimento Materno Infantile e Tecnologie Biomediche, University of Brescia, Brescia, Italy. [4]Hemostasis, Thrombosis, and Vascular Biology Research Group, Hungarian Academy of Sciences, Debrecen, Hungary. [5]Department of Medicine, Division of Nephrology, Hypertension, and Renal Transplantation, University of Florida, Gainesville, Florida, USA. [6]Rural Clinical School, School of Medicine, The University of Queensland, Brisbane, St. Lucia, Australia. [7]École Polytechnique Fédérale de Lausanne (EPFL), Swiss Institute for Experimental Cancer Research (ISREC), Lausanne, Switzerland. [8]Birmingham Veterans Administration Medical Center, Birmingham, Alabama, USA.

Ferritin plays a central role in iron metabolism and is made of 24 subunits of 2 types: heavy chain and light chain. The ferritin heavy chain (FtH) has ferroxidase activity that is required for iron incorporation and limiting toxicity. The purpose of this study was to investigate the role of FtH in acute kidney injury (AKI) and renal iron handling by using proximal tubule–specific *FtH*-knockout mice (*FtH*^PT–/– mice). *FtH*^PT–/– mice had significant mortality, worse structural and functional renal injury, and increased levels of apoptosis in rhabdomyolysis and cisplatin-induced AKI, despite significantly higher expression of heme oxygenase-1, an antioxidant and cytoprotective enzyme. While expression of divalent metal transporter-1 was unaffected, expression of ferroportin (FPN) was significantly lower under both basal and rhabdomyolysis-induced AKI in *FtH*^PT–/– mice. Apical localization of FPN was disrupted after AKI to a diffuse cytosolic and basolateral pattern. FtH, regardless of iron content and ferroxidase activity, induced FPN. Interestingly, urinary levels of the iron acceptor proteins neutrophil gelatinase–associated lipocalin, hemopexin, and transferrin were increased in *FtH*^PT–/– mice after AKI. These results underscore the protective role of FtH and reveal the critical role of proximal tubule FtH in iron trafficking in AKI.

Introduction

Acute kidney injury (AKI) remains a major clinical challenge, with significant attributable morbidity and mortality (1). The pathogenesis of AKI is remarkably complex due to numerous insults as well as the involvement of many independent and overlapping pathophysiological pathways. Given its anatomy and intricate function, the proximal tubule segment of the nephron is predictably the most susceptible to various forms of injury. Multiple molecular mechanisms have been proposed that potentiate and/or aggravate AKI, but ROS-induced kidney injury is recognized as one of the key mediators (2–8). In support of this premise, studies have provided strong evidence that upregulation of endogenous antioxidant defense systems, such as induction of the heme oxygenase-1 (HO-1) enzyme, mitigates AKI in different injury settings (4).

Once liberated into a free catalytic form, iron is an essential mediator of injury that can instigate and maintain generation of ROS that may damage literally all macromolecular cellular compartments. This property is attributed to the ability of iron to readily accept and donate electrons. Although potentially toxic in its free catalytic form, the very same redox potential of iron makes it a requisite for life for almost all organisms. Hence, to maintain a delicate balance among homeostatic needs and to prevent potential detrimental effects, multiple highly synchro-

nized regulatory mechanisms that function at both systemic and cellular levels have evolved. An intriguing, highly conserved molecule that has the capacity of sequestering large amounts of iron (up to 4,500 atoms) in a safe, soluble, and bioavailable form is ferritin. The major regulator of intracellular iron, ferritin is made of 24 subunits of 2 distinct types: heavy chain (H-ferritin; FtH) and light chain (L-ferritin; FtL) (9). Importantly, FtH has ferroxidase activity, which catalyzes the conversion of the ferrous form (Fe^{2+}) to the ferric form (Fe^{3+}), allowing the safe incorporation of iron into the ferritin shell and thereby attenuating participation of free iron in ROS generation. Previous studies have demonstrated that induction of HO-1 is coupled to upregulation of ferritin — the latter a response to sequestration of iron from the HO-1 catalyzed reaction (8, 10). Interestingly, FtH, which was traditionally recognized as a cytosolic protein, has been described in the mitochondria and the nucleus, which highlights its function at diverse cellular organelles (11, 12). Furthermore, recent data suggest that FtH is also involved in functions that are not primarily linked to iron sequestration, such as promotion of angiogenesis and attenuation of osteoblastic differentiation of vascular smooth muscle cells (13, 14).

The detrimental role of iron in AKI has been demonstrated in multiple models of AKI. Furthermore, chelation of iron has been shown to be protective in both in vitro and in vivo models of AKI (2, 3, 5, 15–21). However, despite the recognition of iron as a culprit in AKI, little is known about the nephron's response — to minimize the availability and enhance the redistribution of iron — that could potentially alleviate injury.
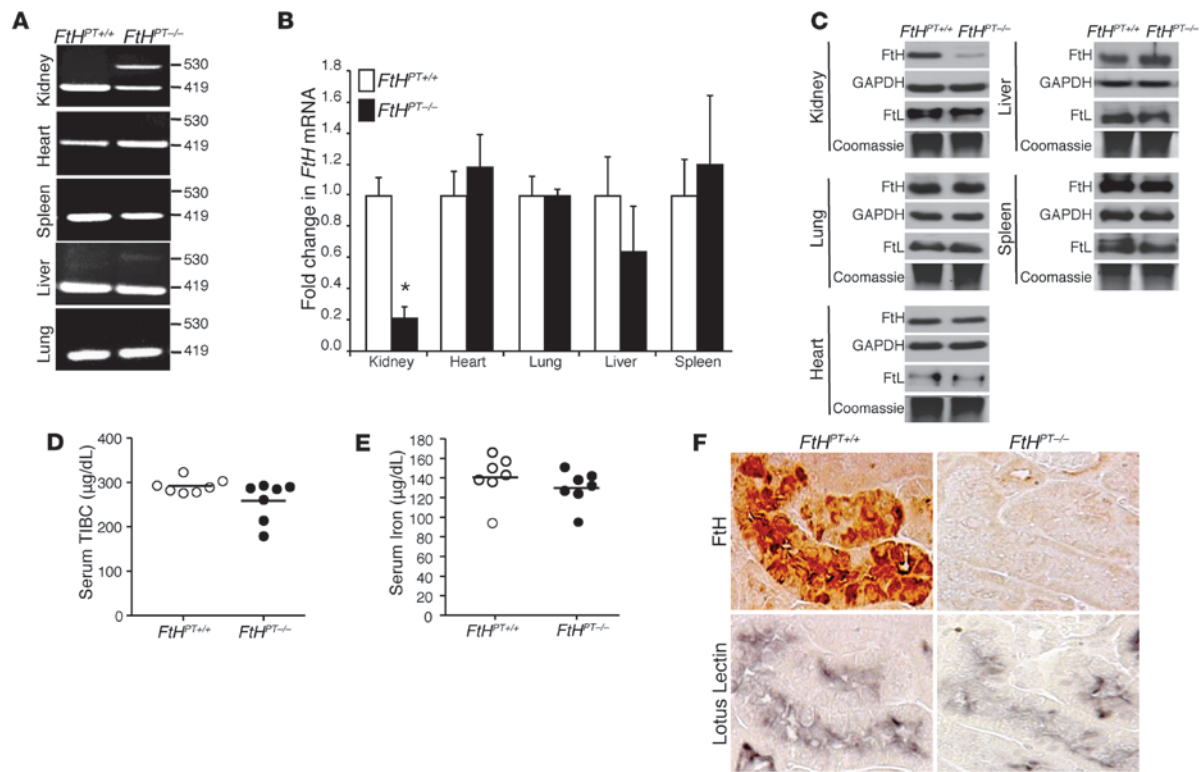
Figure 1

Characterization of *FtH^PT–/–* mice. (**A**) PCR analysis, performed on genomic DNA from organs, for the presence of the floxed (419 bp) and deleted (530 bp) *FtH* allele. (**B**) *FtH* mRNA expression in the organs of *FtH^PT+/+* and *FtH^PT–/–* mice, analyzed by real-time PCR. Results were normalized to GAPDH and expressed as fold change compared with *FtH^PT+/+*. Data are mean ± SEM. *$P < 0.001$ vs. *FtH^PT+/+*. (**C**) Western blot was performed on organ lysates for FtH expression. Membranes were stripped and reprobed for GAPDH as a loading control. Native gels were run for the detection of FtL, and coomassie stain served as a loading control. (**D** and **E**) Total iron-binding capacity (TIBC; **D**) and total iron levels (**E**) in the serum of *FtH^PT+/+* and *FtH^PT–/–* mice. Data are mean ± SEM. No statistical difference was present between groups. (**F**) Immunohistochemical staining on serial kidney sections from *FtH^PT+/+* and *FtH^PT–/–* mice for FtH and the proximal tubule marker lotus lectin. For each experiment, n = 4–8 per group.

Additionally, whereas the contribution of the intestine, liver, and reticuloendothelial system in systemic iron homeostasis is extensively studied, very little is known about the extent of renal involvement in such orchestration (22–28). Considering the wealth of knowledge regarding renal handling of assorted molecules and electrolytes, animal models that would enable deciphering the role of the kidney in systemic iron homeostasis and iron trafficking during AKI are timely and may provide new avenues for potential therapies.

To address these questions, we generated renal proximal tubule–specific FtH–deleted mice (referred to herein as *FtH^PT–/–* mice) to examine the role of FtH in AKI and, more notably, to study the kidney's response to iron trafficking at the renal cellular level under pathological conditions.

Results

Characterization of FtH^PT–/– mice. Renal proximal tubule–specific *FtH* deletion was achieved by crossing *FtH^lox/lox* mice (27) with PEPCK-Cre mice (29). Notably, the Cre mice were generated using a mutated PEPCK promoter, resulting in minimal hepatocyte activity (30). *FtH^PT–/–* mice were born at the expected Mendelian ratio, were viable and fertile, and did not manifest any apparent abnormalities during 6 months of observation. In addition, analysis of kidney sections from these mice did not demonstrate any patho-

logical findings (data not shown). *FtH^lox/lox* mice — homozygous for the floxed allele and expressing FtH in the proximal tubules — were used as controls (referred to herein as *FtH^PT+/+* mice). The recombination event by Cre was confirmed by PCR using genomic DNA with specific primers (Table 1). The recombined product was detected in the kidneys and, to a lesser extent, the livers of *FtH^PT–/–* mice. No recombined product was detected in any of the other organs tested, including heart, spleen, and lung (Figure 1A). This was also validated by mRNA expression analysis of *FtH^PT+/+* and *FtH^PT–/–* organs, with a significant decrease in *FtH* expression in only the kidneys of *FtH^PT–/–* mice (Figure 1B). There were no significant differences in mRNA and protein expression of FtH in whole-liver lysates from *FtH^PT+/+* and *FtH^PT–/–* mice (Figure 1, B and C). Staining for FtH was detectable in the liver, except in a subset of periportal hepatocytes, in which expression was decreased in *FtH^PT–/–* mice (Supplemental Figure 1; supplemental material available online with this article; doi:10.1172/JCI67867DS1). These observations are consistent with the original description of the PEPCK-Cre reporter mice (31). Western blot analysis validated deletion of FtH only in the kidneys of *FtH^PT–/–* mice, with no compensatory increase in FtL expression (Figure 1C). Additionally, under basal conditions, deletion of *FtH* in the proximal tubules was not associated with significant alteration of total iron-binding capacity or serum iron (Figure 1, D and E). Furthermore, while the
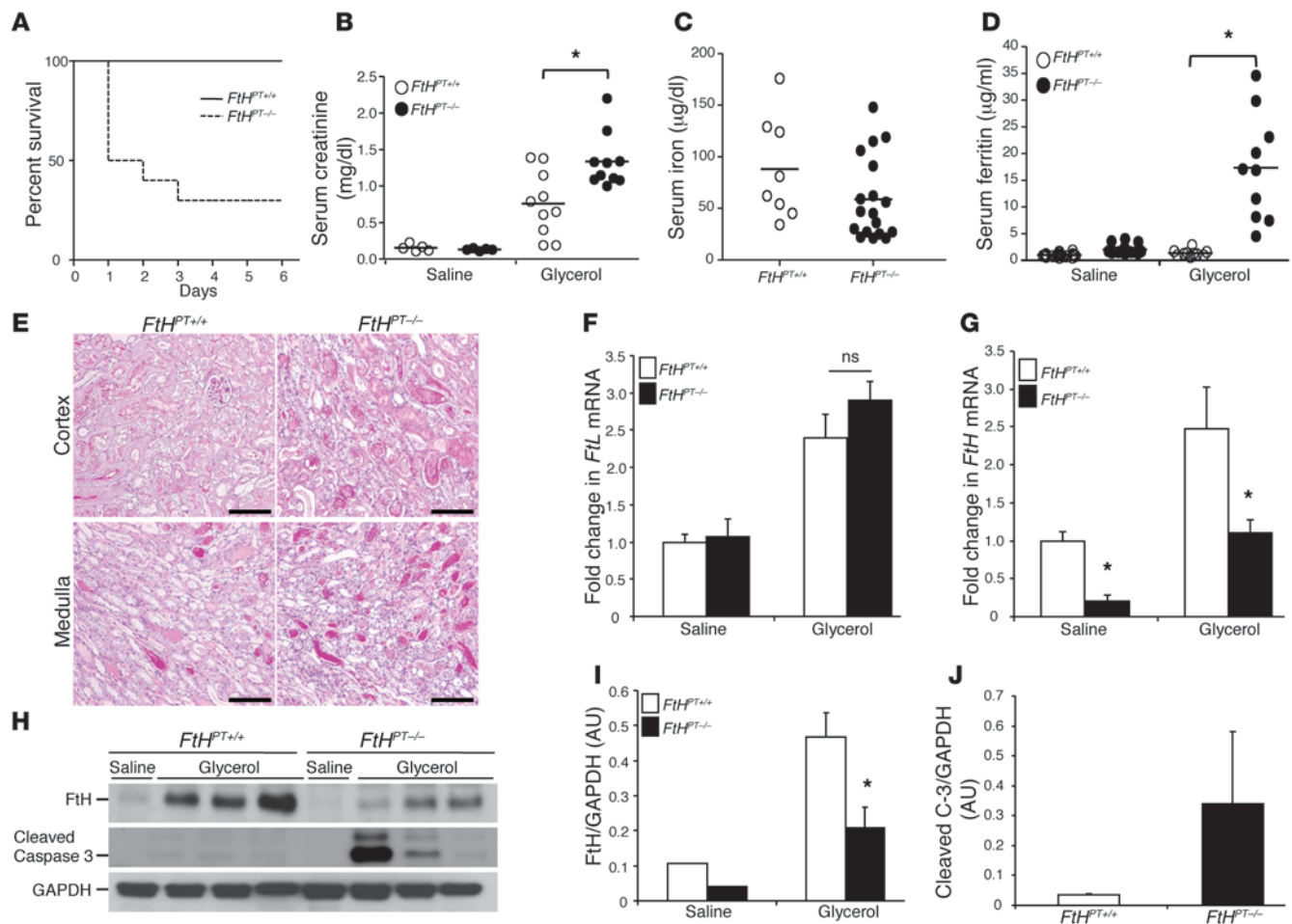
Figure 2
Ablation of FtH in the proximal tubules worsens heme-mediated AKI. (**A**) *FtH$^{PT+/+}$* and *FtH$^{PT–/–}$* mice were administered glycerol, and survival was monitored up to 6 days (*n* = 10 per group). (**B**) Serum creatinine was measured 24 hours after saline or glycerol administration. Data are mean ± SEM. *$P < 0.01$ vs. glycerol-treated *FtH$^{PT+/+}$*. (**C**) Total iron levels in the serum of glycerol-treated *FtH$^{PT+/+}$* and *FtH$^{PT–/–}$* mice. (**D**) Serum ferritin was measured 24 hours after saline or glycerol administration. *$P < 0.01$ vs. glycerol-treated *FtH$^{PT+/+}$*. (**E**) Representative PAS staining of cortex and medulla of glycerol-treated *FtH$^{PT+/+}$* and *FtH$^{PT–/–}$* mice. Scale bar: 100 μm. (**F** and **G**) *FtL* and *FtH* mRNA expression was analyzed by real-time PCR in total RNA extracts of kidneys from saline- or glycerol-treated *FtH$^{PT+/+}$* and *FtH$^{PT–/–}$* mice. Data are expressed as fold change in ferritin expression compared with saline-treated *FtH$^{PT+/+}$* mice (*n* = 3 per group). *$P < 0.01$. (**H**) FtH and cleaved caspase-3 expression was verified by Western blot. Blots were stripped and reprobed for GAPDH. (**I** and **J**) Expression of the indicated proteins in the kidneys was analyzed by densitometry, normalized to GAPDH, and expressed as mean ± SEM. *$P < 0.05$ vs. glycerol-treated *FtH$^{PT+/+}$*.

proximal tubules of *FtH$^{PT+/+}$* mice demonstrated colocalization of FtH expression and the proximal tubule marker lotus lectin after glycerol administration, there was no FtH expression in *FtH$^{PT–/–}$* proximal tubules (Figure 1F).

Proximal tubule FtH deletion aggravates heme-mediated AKI. Given the significance of FtH in the safe sequestration of the potentially detrimental iron, we hypothesized that deletion of FtH in proximal tubules of the kidney would aggravate heme-mediated AKI in a model of glycerol-induced rhabdomyolysis. To this end, we demonstrated that glycerol administration to *FtH$^{PT–/–}$* mice led to substantial mortality compared with *FtH$^{PT+/+}$* controls (Figure 2A). To determine the functional significance of *FtH* deletion in proximal tubules, we measured serum creatinine 24 hours after glycerol administration. Whereas there was no significant difference in creatinine levels after saline administration, the rise in serum creatinine in response to rhabdomyolysis-induced AKI was significantly higher in *FtH$^{PT–/–}$*

versus *FtH$^{PT+/+}$* mice (Figure 2B). In addition, although serum iron levels were not significantly different between the groups (Figure 2C), serum ferritin levels were markedly higher in *FtH$^{PT–/–}$* versus *FtH$^{PT+/+}$* mice after glycerol administration (Figure 2D). Renal histology further corroborated the protective role of FtH in AKI, as evidenced by the higher number of tubular casts and necrotic tubules and the loss of proximal tubule brush border in *FtH$^{PT–/–}$* kidneys after glycerol administration (Figure 2E). In order to evaluate the role of ferritin as a protective response to AKI, we further examined the kidneys for *FtL* and *FtH* expression, both of which increased markedly after glycerol administration (Figure 2, F and G). *FtH* levels were significantly lower in *FtH$^{PT–/–}$* mice (Figure 2G). This was also confirmed by Western blot on whole kidney lysates from saline- and glycerol-treated animals (Figure 2, H and I). In addition, we found that expression of cleaved caspase-3, a marker of apoptosis, was higher in *FtH$^{PT–/–}$* kidneys after rhabdomyolysis (Figure 2, H and J).
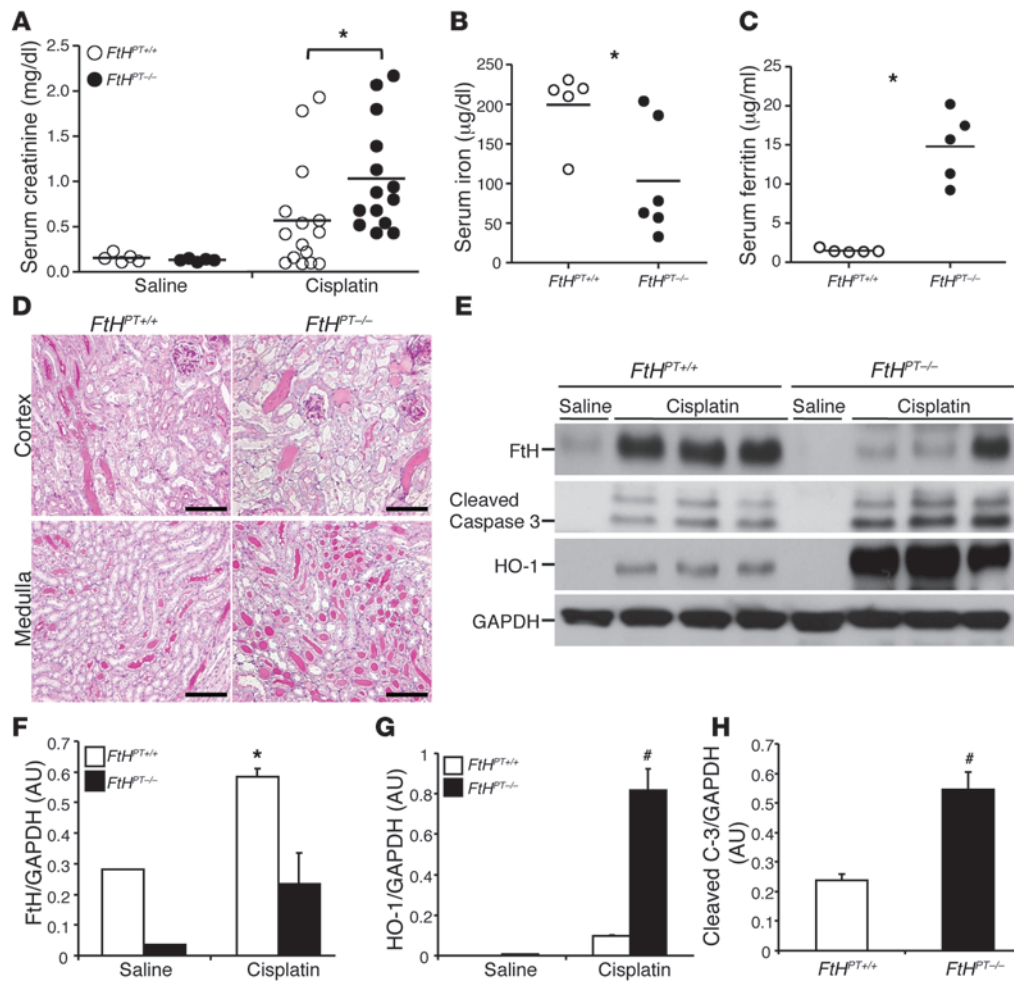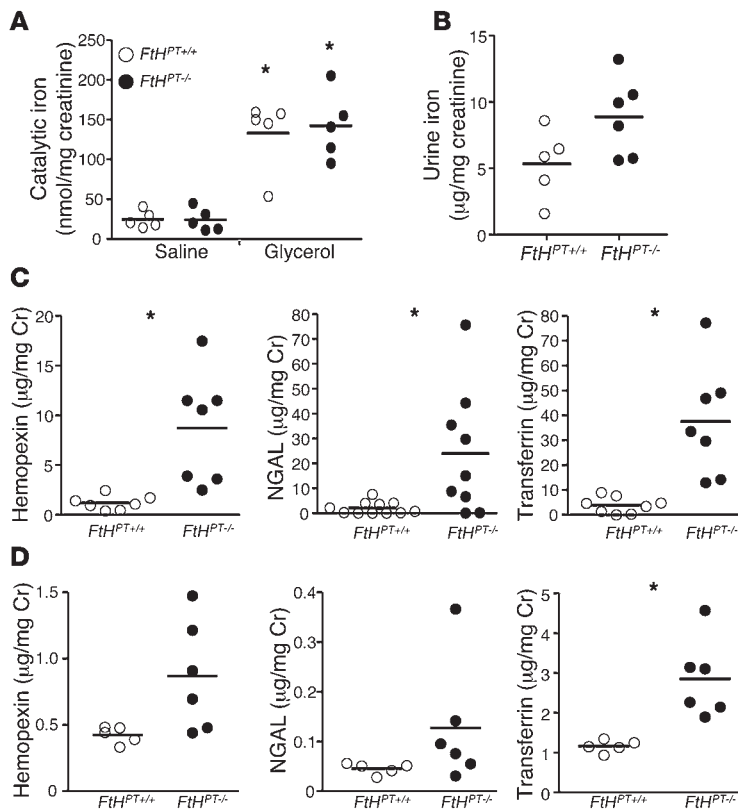
Figure 3
Cisplatin nephrotoxicity is exacerbated in the absence of proximal tubule FtH expression. Mice were administered saline or cisplatin for 3 days ($n = 3$–10 per group). (**A**) Serum creatinine, measured at time of harvest and expressed as mg/dl. *$P < 0.05$ vs cisplatin-treated $FtH^{PT+/+}$. (**B**) Total iron levels in the serum of $FtH^{PT+/+}$ and $FtH^{PT-/-}$ mice after cisplatin administration. *$P < 0.05$ vs. $FtH^{PT+/+}$. (**C**) Serum ferritin in cisplatin-treated $FtH^{PT+/+}$ and $FtH^{PT-/-}$ mice. *$P < 0.01$ vs $FtH^{PT+/+}$. (**D**) Representative PAS staining of cortex and medulla of saline- or cisplatin-treated $FtH^{PT+/+}$ and $FtH^{PT-/-}$ mice. Scale bar: 100 μm. (**E**) FtH, cleaved caspase-3, and HO-1 expression was verified by Western blot. Blots were stripped and reprobed for GAPDH. (**F**–**H**) Expression of the indicated proteins in the kidneys was analyzed by densitometry, normalized to GAPDH, and expressed as mean ± SEM. *$P < 0.05$, #$P < 0.01$ vs. cisplatin-treated $FtH^{PT+/+}$.

Proximal tubule FtH deletion exacerbates non–heme-mediated AKI. To elucidate the protective role of FtH in a primarily non–heme-dependent injury setting, we used another model of AKI, namely cisplatin nephrotoxicity. At 3 days after cisplatin administration, $FtH^{PT-/-}$ mice had significantly higher serum creatinine and ferritin levels, which were associated with a significant decrease in serum iron levels, compared with $FtH^{PT+/+}$ mice (Figure 3, A–C). Concurrently, $FtH^{PT-/-}$ mice exhibited worse structural architecture, with a substantial number of casts and necrotic tubules (Figure 3D). Consistent with previous observations (8), FtH was induced after cisplatin administration in $FtH^{PT+/+}$ mice, but this was significantly lower in $FtH^{PT-/-}$ mice (Figure 3, E and F). Western blot analysis revealed higher cleaved caspase-3 expression in $FtH^{PT-/-}$ kidneys compared with cisplatin-treated $FtH^{PT+/+}$ mice (Figure 3, E and H). Interestingly, we found that expression of HO-1, a cytoprotective enzyme indispensable for protection against both glycerol- and

cisplatin-induced kidney injury, was significantly higher under injury settings (Figure 3E), but nonetheless was unable to provide renal protection in the absence of FtH. Taken together, these results indicate that proximal tubule FtH expression and induction plays an important protective role in different settings of AKI.

Urinary iron acceptor proteins are increased in the absence of proximal tubular FtH. To investigate the response of the nephron to increased levels of iron, we measured levels of urinary catalytic iron. While there was a significant increase in catalytic iron levels after glycerol administration, such increment was not significantly altered by proximal tubule FtH ablation (Figure 4A). However, total urinary iron levels tended to be higher in the $FtH^{PT-/-}$ mice after glycerol-induced rhabdomyolysis (Figure 4B). In light of the evidence that total urinary iron was higher while there was no difference in catalytic iron, we sought to determine the levels of neutrophil gelatinase-associated lipocalin (NGAL; an iron siderophore

Figure 4
Increased excretion of urinary iron and iron acceptor proteins in $FtH^{PT-/-}$ mice after AKI. (**A**) Catalytic iron was measured in the urine of saline- or glycerol-treated $FtH^{PT+/+}$ and $FtH^{PT-/-}$ mice. Data were normalized to urine creatinine levels and expressed as nanomoles of iron per milligram creatinine. *$P < 0.05$ vs. respective saline control. (**B**) Total iron content was measured in the urine of glycerol-treated $FtH^{PT+/+}$ and $FtH^{PT-/-}$ mice. Data were normalized to urine creatinine and expressed as microgram iron per milligram creatinine. (**C** and **D**) Hemopexin, NGAL, and transferrin were measured by ELISA in the urine from glycerol- (**C**) or cisplatin-treated (**D**) $FtH^{PT+/+}$ and $FtH^{PT-/-}$ mice. Data were normalized to urine creatinine and expressed as microgram per milligram creatinine. *$P < 0.05$ vs. $FtH^{PT+/+}$.

that increases after AKI), transferrin, and hemopexin as potential iron acceptor proteins. As shown in Figure 4C and Supplemental Figure 2, A and B, hemopexin, NGAL, and transferrin levels were significantly higher in the urine from $FtH^{PT-/-}$ mice with rhabdomyolysis, both with and without normalization of these levels to urine creatinine. After cisplatin administration, all 3 urinary iron acceptors tended to be higher in $FtH^{PT-/-}$ than in $FtH^{PT+/+}$ mice (Figure 4D and Supplemental Figure 2D). However, after normalization to creatinine, only transferrin levels were significantly higher (Figure 4D). Under basal conditions, levels of NGAL ($FtH^{PT+/+}$, 2.4 ± 1 ng/mg Cr; $FtH^{PT-/-}$, 1.6 ± 0.1 ng/mg Cr), hemopexin ($FtH^{PT+/+}$, 3.17 ± 0.3 ng/mg Cr; $FtH^{PT-/-}$, 3.8 ± 0.1 ng/mg Cr), and transferrin ($FtH^{PT+/+}$, 0.96 ± 0.16 ng/mg Cr; $FtH^{PT-/-}$, 1.2 ± 0.13 ng/mg Cr) were not significantly different between the groups ($n = 5$–8 per group). These results suggest that the kidney plays an important role in iron trafficking and homeostasis during injury.

FtH modulates expression of FPN, but not DMT-1, during AKI. We next examined the expression of the known iron-trafficking proteins divalent metal transporter 1 (DMT-1) and ferroportin (FPN) in response to injury. DMT-1 was induced after AKI in both $FtH^{PT+/+}$ and $FtH^{PT-/-}$ kidneys to similar levels in the cisplatin and rhabdomyolysis models (Supplemental Figure 3A). In contrast, we found that while FPN expression was significantly induced in the cortex and medulla after rhabdomyolysis-induced AKI, both mRNA and protein levels of FPN were markedly lower in $FtH^{PT-/-}$ mice compared with their $FtH^{PT+/+}$ littermates under both basal and injury settings (Figure 5, A and B). Of note, there was no detectable change in hepatic expression of FPN in $FtH^{PT-/-}$ mice (Supplemental Figure 1). Under basal conditions, FPN was predominantly expressed in the apical brush border region of the

proximal tubules in the outer stripe of the medulla and inner cortical areas of the kidney (Figure 5, C–E, and Supplemental Figure 4, A and B). The brush border localization of FPN in renal proximal tubules was also confirmed by immunogold electron microscopy (Figure 5C). Occasional gold particles were found in the mitochondria and cytoplasm of renal proximal tubules, whereas experimental controls without the primary antibody did not demonstrate any nonspecific immunogold localization (Supplemental Figure 4, C and D). A few renal tubules in the outer cortex of uninjured kidneys showed cytoplasmic and basolateral FPN expression (Supplemental Figure 4, A and B). Upon injury, the apical localization of FPN in the basal state was markedly altered to a diffuse cytosolic and basolateral pattern and extended to the outer cortex of the kidney (Figure 5, D and E). In addition, after injury, induction of FtH was accompanied by a substantial increase in FPN expression in the proximal tubules of $FtH^{PT+/+}$ mice (Figure 5, B and D). Serial sections revealed overlap in staining of FtH and FPN in the same renal tubules (Figure 5E).

FtH regulates FPN expression in renal proximal tubules. Upon further investigation of the relationship between FtH and FPN, we determined that $HO-1^{-/-}$ mice had increased FtH expression along with increased FPN levels in the kidneys (Figure 6, A and B). Such co-induction of FPN and FtH may explain the aberrant iron deposition in proximal tubules of $HO-1^{-/-}$ kidneys. To further decipher the mechanism of FPN modulation by FtH, we isolated proximal tubular cells from wild-type mice and administered apoferritin (ferritin shell, devoid of iron). FPN expression was induced after apoferritin administration at the mRNA and protein levels (Figure 6, C and D). As apoferritin is a combination of both FtH and FtL, we treated cells with recombinant FtH alone and
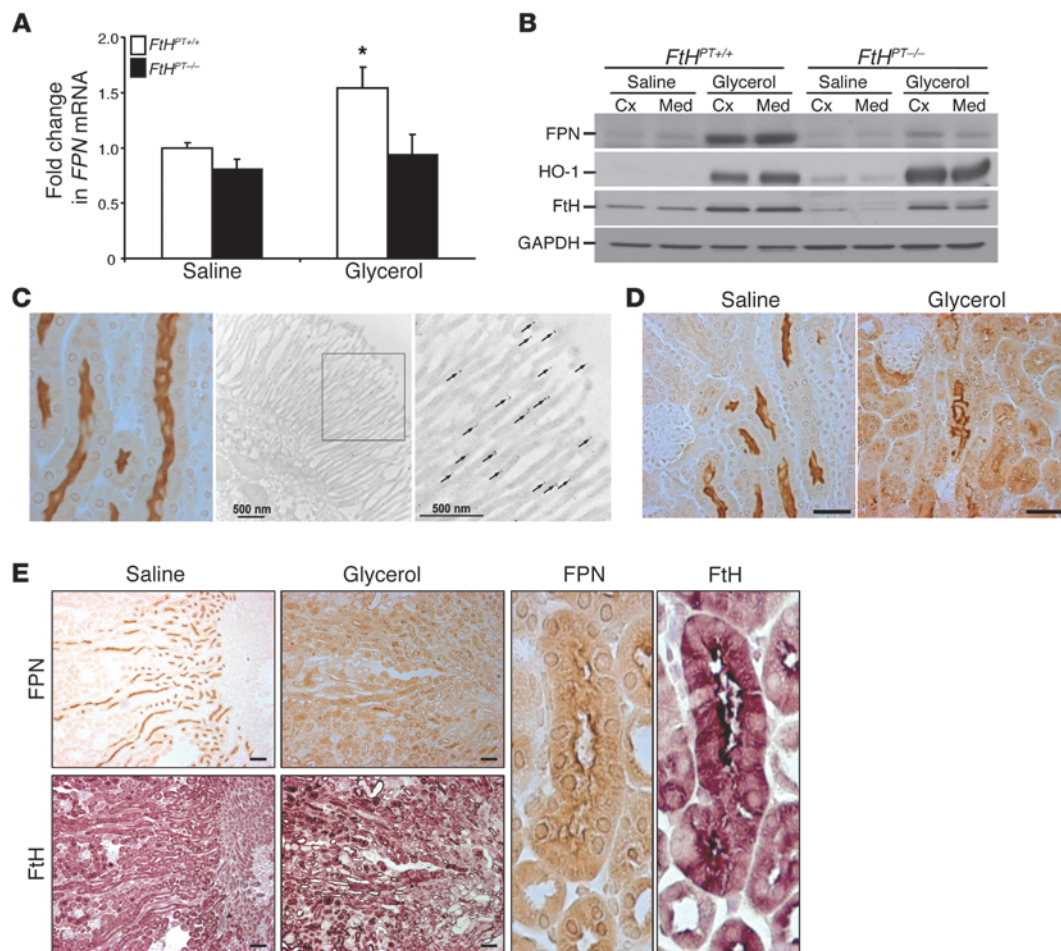
Figure 5
FtH modulates FPN expression during AKI. (**A**) FPN expression in *FtHPT+/+* and *FtHPT–/–* kidneys after saline or glycerol administration, examined by real-time PCR. Data were normalized to GAPDH and expressed as fold change in *FPN* mRNA relative to saline-treated *FtHPT+/+* (*n* = 3–5 per group). *$P < 0.05$. (**B**) FPN, HO-1, and FtH expression in the cortex and medulla of *FtHPT+/+* and *FtHPT–/–* mice, analyzed by Western blot. Membranes were probed for GAPDH as a loading control. (**C**) Immunohistochemical staining of a kidney section for FPN and immunoelectron micrograph of a proximal tubule in the outer stripe of the outer medulla, illustrating FPN localization to the brush border on the apical surface. Arrows indicate gold particles. (**D**) Immunohistochemical staining showing differential expression of FPN in the proximal tubules of saline- and glycerol-treated *FtHPT+/+* mice. (**E**) Immunohistochemical staining of serial kidney sections for FPN and FtH after administration of saline or glycerol, as well as magnified views showing their colocalization in the proximal tubule (right, enlarged ×10). Scale bars: 500 nm (**C**); 500 nm (**C**, inset); 100 μm (**D** and **E**).

observed an increase in FPN expression. Furthermore, a mutant form of ferritin lacking ferroxidase activity (referred to herein as FtH-M) was also able to induce FPN (Figure 6E). These results demonstrated ferritin-mediated induction of FPN in renal proximal tubular cells and corroborate our in vivo findings of increased FPN expression in *FtHPT+/+* kidneys after AKI (Figure 5B). Conversely, the absence of FtH in *FtHPT–/–* kidneys was associated with decreased FPN expression (Figure 5B).

We further assessed the ability of proximal tubular cells to mediate iron trafficking via a FPN-dependent mechanism. Cells were plated on Transwell filters, and polarization was confirmed by staining cells for ZO-1, an apical peripheral membrane protein associated with tight junctions (Figure 6F). Consistent with previous studies using hepatocytes (32), hepcidin decreased the expression of FPN in proximal tubular epithelial cells in a time-dependent manner (Figure 6G), and pretreatment with hepcidin significantly reduced

uptake of apical radiolabeled iron chloride (^{55}Fe) by approximately 35% (Figure 6H), which suggests that iron import in renal proximal tubular cells is mediated, at least in part, via FPN.

Discussion

In this study, we found that *FtHPT–/–* mice, with conditional deletion of *FtH* in renal proximal tubules, demonstrated increased susceptibility to injury manifested by worse renal structural and functional measures in 2 different models of AKI: rhabdomyolysis and cisplatin nephrotoxicity. Our results validated that the proximal tubules are the major site of FtH expression and verified the detrimental role of iron in AKI. Moreover, we found that while FtH ablation was accompanied by decreased FPN expression in vivo, addition of apoferritin to proximal tubular cells in vitro resulted in a significant increase in FPN expression at both mRNA and protein levels. Furthermore, we demonstrated that the ferroxidase
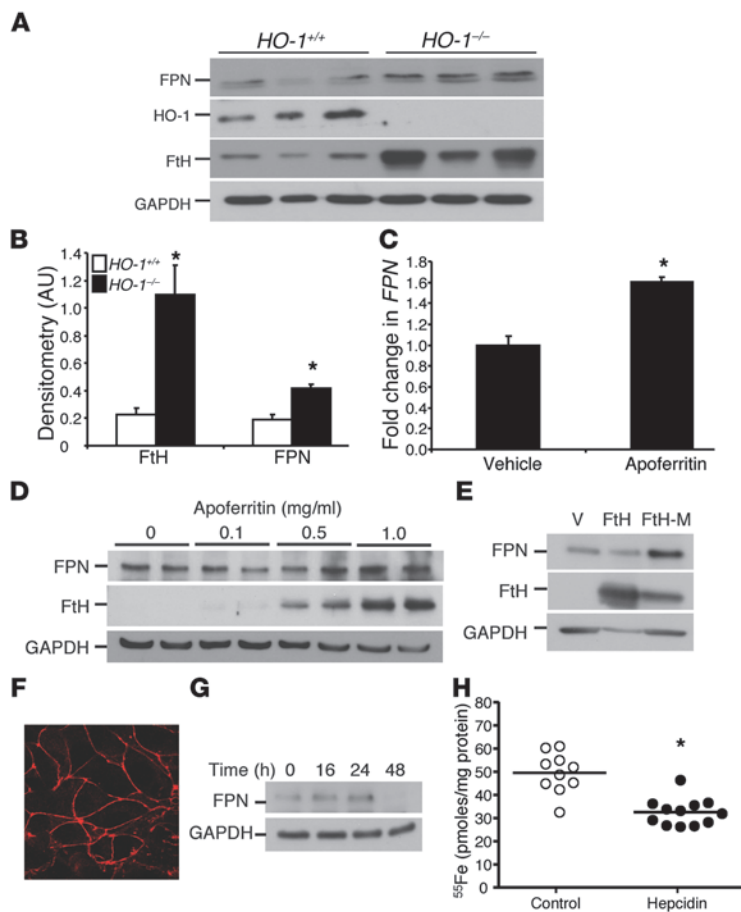
Figure 6
FtH regulates FPN expression in renal proximal tubules. (**A**) Whole kidney lysates from *HO-1⁺/⁺* and *HO-1⁻/⁻* mice were analyzed for FPN, HO-1, and FtH levels by Western blot. Membranes were reprobed for GAPDH to demonstrate equal loading. (**B**) Kidney FPN and FtH expression was analyzed by densitometry analysis, normalized to GAPDH, and expressed as mean ± SEM. *$P < 0.05$ vs *HO-1⁺/⁺*. (**C**) *FtH^PT+/+* proximal tubular epithelial cells were treated in vitro with apoferritin for 8 hours and analyzed for *FPN* expression by real-time PCR. Data are expressed as fold change relative to vehicle-treated cells. *$P < 0.05$. (**D**) Proximal tubular epithelial cells were treated with the indicated doses of apoferritin for 16 hours and analyzed for FPN and FtH expression by Western blot. GAPDH served as a loading control. (**E**) Proximal tubular epithelial cells were treated with vehicle, FtH, or FtH-M for 16 hours and analyzed for FPN and FtH expression by Western blot. GAPDH served as a loading control. Results are representative of 3 independent experiments. (**F**) Immunocytochemistry for ZO-1 expression on cells grown on Transwell filters, confirming polarization. Original magnification, ×180. (**G**) Proximal tubular epithelial cells were treated with hepcidin for the indicated times and analyzed for FPN expression by Western blot. (**H**) Proximal tubular cells grown on Transwell filters were pretreated with vehicle (control) or hepcidin for 48 hours, ⁵⁵Fe was administered to the apical compartment for 2 hours, and cellular ⁵⁵Fe levels were measured and expressed as picomoles of iron per milligram protein. *$P < 0.05$ vs. control.

activity of FtH was not essential in upregulation of FPN expression. Our results also highlighted that loss of FtH in the proximal tubules did not lead to a compensatory increase in FtL levels, as has been observed in the liver (27). This suggests that while the kidney is actively involved in iron trafficking and reabsorption, it is not a major site of iron storage under physiological conditions.

The toxicity of excess iron deposition in different tissues has been recognized in clinical conditions, such as systemic hemochromatosis. However, the implications of catalytic iron in AKI pathogenesis in the absence of systemic iron overload have only recently begun to emerge. Several studies have reported that iron is deleterious in multiple settings of AKI, such as rhabdomyolysis, nephrotoxicity (cisplatin and gentamycin), ischemia/reperfusion injury, and contrast-induced AKI. Furthermore, iron chelation with deferoxamine has been reported to provide protection and significantly improve the severity and outcomes of AKI (2, 3, 5, 15–21, 33). Additionally, other endogenous proteins involved in iron regulation and chelation, such as hepcidin and NGAL, have been shown to protect against AKI (21, 34–37). Our current findings corroborate the injurious role of iron in AKI and delineate the renal proximal tubule as the major site of iron-induced injury.

The nephron has the capacity to limit the deleterious effects of AKI via different mechanisms. HO-1 is an enzyme that is rapidly induced in response to a variety of injurious stimuli, providing potent antioxidant, antiinflammatory, and antiapoptotic effects. The protective effects of HO-1 have been extensively studied, and its induction is known to be beneficial in a wide range of AKI

settings (4, 7). Additionally, HO-1 induction was coupled to increased ferritin expression during AKI (8, 10). Consistent with recent findings in the intestine, our results revealed that deletion of FtH was accompanied by a significant increase in HO-1 expression under both basal and AKI conditions, presumably as an antioxidant compensatory mechanism (24). However, despite significantly higher levels of HO-1 in *FtH^PT−/−* kidneys, AKI severity was remarkably higher in these animals compared with their control littermates. These findings demonstrated that the beneficial effects of HO-1 are codependent on FtH and underscored the importance of FtH induction as a key antioxidant mechanism in proximal tubules during AKI.

Control of iron metabolism is a meticulously regulated process to provide iron when needed and curtail its toxicity by restricting availability of free iron. At the systemic level, this is mainly achieved by vigilant pathways of iron absorption and recycling, namely, release of iron from macrophages, release of stored iron from hepatocytes, and absorption of dietary iron by duodenal enterocytes (23, 38, 39). In this regard, the only known membrane iron transporter, FPN, is at the epicenter of this axis, and its aberrant expression has previously been shown to cause derangements in systemic iron homeostasis (40, 41). Several studies have demonstrated that expression of FPN is regulated at multiple levels, including a posttranslational mechanism by hepcidin, a generally accepted major pathway for FPN regulation. Hepcidin is primarily produced and secreted by hepatocytes and functions by directly binding to FPN, causing its internalization and degradation in lysosomes (25, 40–42).

research article
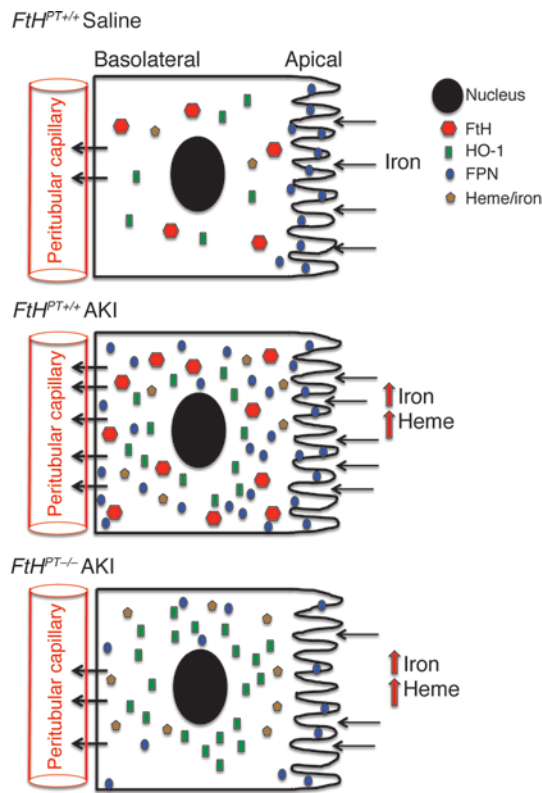
Figure 7
Regulation of iron homeostasis by FtH in the proximal tubules of the kidney. Under basal conditions, FPN is expressed on the apical surface of the proximal tubules, which facilitates iron reabsorption and safe sequestration by ferritin. AKI induces the expression of FtH and HO-1, and FtH in turn increases expression and redistribution of FPN throughout the tubule and toward the basolateral side. In the absence of *FtH*, FPN induction after AKI is reduced and may potentially impair iron reabsorption. Although HO-1 is substantially increased, these cells are more susceptible to injury and apoptosis, which suggests that HO-1–mediated protection is dependent on FtH.

Despite extensive research in the field of iron metabolism, little is known about the contributing role of FPN in the kidney. Emerging data, however, suggest that the kidney may be more extensively involved in iron metabolism than initially proposed. For instance, studies have revealed that multiple proteins involved in iron metabolism are expressed in the kidney, including hepcidin, FPN, and DMT-1 (43–47). Intriguingly, we found that deletion of FtH did not affect the expression of DMT-1 (expressed in late endosome/lysosome membranes of tubular cells), but was accompanied with diminution of FPN expression, in $FtH^{PT-/-}$ kidneys. This decrease was observed at both mRNA and protein levels, suggesting the correlation to be hepcidin independent. Furthermore, we observed that rhabdomyolysis-induced AKI was associated with significant induction of FPN expression in $FtH^{PT+/+}$ kidneys and, to a lesser extent, $FtH^{PT-/-}$ kidneys. Under normal conditions, FPN was predominantly expressed at the apical side of the proximal tubule. However, after AKI, FPN was redistributed to a cytosolic and basolateral pattern in proximal tubules. To clarify whether FPN expression is mediated by iron and/or ferritin, we used apoferritin and recombinant FtH and FtH-M, the latter of which lacks

ferroxidase activity. These experiments revealed that apoferritin and FtH (both devoid of iron) significantly increased FPN expression. In addition, our observations suggest that the ferroxidase activity of FtH was not required in this regulatory mechanism. Therefore, we report for the first time a novel function for FtH in the context of regulation of FPN expression.

The mechanism of such regulation may provide new avenues for better understanding of molecular and systemic iron homeostasis and will require further investigation. FtH is capable of inducing several genes, including iNOS and IL-1β, through modulation of MAPK and NF-κB signaling pathways (48). IL-1β–dependent transcriptional induction of FPN also requires activation of the NF-κB and MAPK pathways (49). Another plausible mechanism may involve the ability of FtH to translocate to the nucleus. While FtH was traditionally regarded as a cytoplasmic protein, its presence in nuclei of different cell types has been previously described (50–52). Furthermore, FtH has been shown to regulate transcription of certain genes, including the human β-globin gene by binding to the highly conserved CAGTGC motif in the promoter (52). The localization of FtH to the nucleus, and its involvement in transcription via modulation of signal transduction and/or regulation of signaling pathways, are potential mechanisms by which FtH may regulate the transcription of FPN. We also suggest that these findings are quite relevant to perceptions regarding the fate of iron released from the heme tetrapyrrole ring by HO in the injured kidney. Such iron is conventionally handled by either 1 of 2 discrete, noninteracting pathways, namely, sequestration by ferritin or trafficking by FPN. Our present data demonstrated that these pathways are indeed linked because of the inductive effect of ferritin on FPN. This inductive effect makes for more efficient cellular handling of iron, a potentially cytotoxic species, especially in the acutely injured kidney.

Although FPN expression was lower in $FtH^{PT-/-}$ kidneys under both basal and AKI conditions, urinary catalytic iron levels were not significantly different between the 2 groups. These results could be explained by higher levels of urinary iron-binding proteins, including NGAL, hemopexin, and transferrin, in $FtH^{PT-/-}$ mice. The presence of iron acceptor proteins in the urine under uninjured conditions may imply that small amounts of such proteins are filtered, and their subsequent increase after AKI reflects the extent of tubular injury and hence decreased reabsorption. This may, however, serve as a protective phenomenon that would minimize the level of intratubular free iron released into the tubules after cell injury and increased delivery. In addition, serum iron levels were significantly lower in $FtH^{PT-/-}$ mice that received cisplatin, but were not different between the groups after glycerol administration. This highlights the difference in the mode of injury inflicted by these models of injury, where rhabdomyolysis predominantly imposes a large heme-iron burden.

Another observation that supports a role of the kidney in systemic iron homeostasis comes from $HO-1^{-/-}$ mice. Although it is well known that HO-1 deficiency leads to iron overload in the kidney, particularly in proximal tubular cells, the precise mechanism of this finding, and whether it may explain the microcytic anemia that accompanies HO-1 deficiency, has not been investigated (48–50). Interestingly, FPN colocalized with FtH, which suggests a role for this protein in iron import. While further studies are required to elaborately substantiate the mechanism of iron overload in $HO-1^{-/-}$ kidneys and its potential involvement in iron deficiency anemia, our results suggest that the higher levels of FtH expression and the subsequent increase in FPN may explain the deranged iron deposition in kidneys of these animals. We demonstrated that under basal con-

Table 1
Primers for genotyping and real-time PCR analysis

Gene	Primer sequence
Genotyping	
FtH flox forward	5′-CCATCAACCGCCAGATCAAC-3′
FtH flox reverse	5′-CGCCATACTCCAGGAGGAAC-3′
FtH deletion forward	5′-GGCTGTTGTCCTGCTCTAAG-3′
Cre forward	5′-GCCAGGCGTTTTCTGAGCATAC-3′
Cre reverse	5′-CACCATTGCCCCTGTTTCACTATC-3′
Real-time PCR	
FPN forward	5′-GTGGAGTACTTCTTGCTCTGG-3′
FPN reverse	5′-CTGCTTCAGTTCTGACTCCTC-3′
HO-1 forward	5′-GGTGATGGCTTCCTTGTACC-3′
HO-1 reverse	5′-AGTGAGGCCCATACCAGAAG-3′
GAPDH forward	5′-ATCATCCCTGCATCCACT-3′
GAPDH reverse	5′-ATCCACGACGGACACATT-3′
FtL forward	5′-CGTCTCCTCGAGTTTCAGAAC-3′
FtL reverse	5′-CTCCTGGGTTTTACCCCATTC-3′
FtH forward	5′-CCATCAACCGCCAGATCAAC-3′
FtH reverse	5′-GAAACATCATCTCGGTCAAA-3′

ditions, FPN was expressed on the apical membrane of the proximal tubules and facilitated iron reabsorption, which was significantly reduced by hepcidin pretreatment. However, renal iron uptake is not only dependent on FPN, but may likely involve other proteins, such as DMT-1 and transferrin (44, 47, 51).

FtH induction during AKI increases FPN expression and redistributes FPN throughout the tubule and toward the basolateral side, perhaps in an attempt to return iron to the systemic circulation. This notion is supported by a decrease in FPN expression in $FtH^{PT-/-}$ mice, which is accompanied by increased urinary iron excretion (Figure 7). We hypothesize that FPN imports any free iron that may have been filtered into the proximal tubule, thereby preventing the loss of iron and preserving iron homeostasis; the imported Fe^{2+} may be converted to Fe^{3+} by FtH in the intracellular space. However, during AKI and after intracellular iron increases, the directionality may change to minimize injury. It has previously been reported that proximal tubules are capable of FtH secretion, a function that may provide ferroxidase activity within the lumen to convert Fe^{2+} to Fe^{3+} (52). Our model thus posits bidirectionality in the conveyance of iron by FPN, depending on the presence of kidney injury: in states of health, there is net cellular import of iron by FPN into the proximal tubule, whereas in the acutely injured kidney, net extracellular export by FPN mitigates elevations in cellular iron that may otherwise occur.

In conclusion, conditional deletion of *FtH* in kidney proximal tubules led to significantly worse structural and functional AKI. Our results highlighted the key determinant role of iron in 2 models of AKI. Furthermore, our evidence identified proximal tubule FtH as a major regulator of iron and FPN, a function that may provide important clues to derangements in iron homeostasis commonly observed with kidney dysfunction. Based on our observations, we suggest that the kidney plays a crucial role in iron trafficking, particularly during injury, and that additional studies are warranted to gain further insights on the meticulous axis of iron metabolism and involvement of the kidney in this process.

Methods

Animals. The $FtH^{PT+/+}$ mice used in this study were previously described *FtH*-floxed mice (27). PEPCK Cre transgenic mice that express Cre recombinase primarily in the proximal tubules of the kidney were provided by V. Haase (Vanderbilt University, Nashville, Tennessee, USA; ref. 29). All *FtH* transgenic mice used in this study were on a predominantly C57BL/6 background. Adult male mice (8 weeks of age) were provided acidified water (0.3 M ammonium chloride) for 1 week to enhance PEPCK promoter activity in the kidney. $HO-1^{+/+}$ and $HO-1^{-/-}$ male mice (24–26 weeks of age) were used in this study (50).

Confirmation of FtH deletion by genomic DNA PCR. Genomic DNA was isolated from the tail, kidney, heart, spleen, liver, and lung of $FtH^{PT+/+}$ and $FtH^{PT-/-}$ mice using Puregene Core Kit A (Qiagen) according to the manufacturer's instructions. PCR was performed on the genomic DNA to verify the presence of the transgene using specific primers (Table 1). The floxed allele amplicon was identified as 419 bp, while the Cre-mediated deleted allele was 530 bp.

Quantification of mRNA expression. Total RNA was isolated from cells or tissues by TRIZOL (Invitrogen), and SYBR Green–based real-time PCR was performed on cDNA product generated from total RNA (Qiagen). Relative mRNA expression was quantified using the $\Delta\Delta Ct$ method and normalized to *GAPDH* mRNA as an internal control. See Table 1 for real-time primers used. All reactions were performed in triplicate, and specificity was monitored using melting curve analysis.

Cisplatin nephrotoxicity. Cisplatin injury was induced in age-matched $FtH^{PT+/+}$ and $FtH^{PT-/-}$ mice (10–14 weeks of age) as described previously (53). Briefly, mice were administered cisplatin (1.0 mg/ml solution in sterile normal saline) or vehicle (normal saline) at 20 mg/kg body weight by a single intraperitoneal injection. All animals were sacrificed 72 hours after injection, and kidneys were harvested for staining or protein analysis. Blood was collected via cardiac puncture, and serum was isolated for creatinine measurement by LC-MS/MS (54).

Rhabdomyolysis. Glycerol model of rhabdomyolysis was induced in age-matched $FtH^{PT+/+}$ and $FtH^{PT-/-}$ mice as described previously (55). Briefly, mice were deprived of water for 16 hours prior to glycerol administration. Mice were anesthetized with isoflurane and injected with either 50% glycerol in water or saline as a control, 7.5 ml/kg body weight, with half the volume delivered into each anterior thigh muscle. Mice were sacrificed 1 day after injection, and kidneys were harvested for mRNA and protein analysis or embedded in paraffin for staining. Blood was collected via cardiac puncture, and serum was isolated for creatinine measurement. Survival studies were performed in additional $FtH^{PT+/+}$ and $FtH^{PT-/-}$ mice (*n* = 10 per group).

Serum iron, total iron-binding capacity, and urinary iron. Serum iron and total iron-binding capacity were measured using an Alfa Wassermann ACE Axcel clinical chemistry system (West Caldwell). Total urinary iron was measured with a Quantichrome iron assay kit (BioAssay systems) following the manufacturer's instructions. Catalytic iron was measured using previously described methods (18, 56).

Immunohistochemistry. Tissues were embedded in paraffin, sectioned, and stained with periodic acid-Schiff reagent (PAS) using standard protocols. For immunohistochemistry, paraffin-embedded 5-μm kidney sections were deparaffinized in xylenes, rehydrated in a series of ethanol rinses from 100% to 70% ethanol, then washed in distilled water. Antigen retrieval was performed in Trilogy (Cell marque) at 95°C for 30 minutes. Sections were allowed to cool slowly, washed in distilled water, and incubated in 3% H_2O_2 for 10 minutes. Sections were blocked in blocking buffer containing 5% goat serum in PBS, 0.1% Tween-20 (PBST), at room temperature for 1 hour. Primary antibodies were diluted in the blocking buffer for FtH (Santa Cruz Biotechnology; 1:200) or FPN (Abcam; 1:100) and added to sections overnight at 4°C. Sections were washed 3 times with PBST for 5 minutes each. Goat anti-rabbit secondary antibody (Jackson

research article

ImmunoResearch Laboratories; 1:500) was diluted in blocking buffer and added to the sections for 1 hour at room temperature. Sections were washed 3 times with PBST for 5 minutes each. Chromogen substrates were mixed per the manufacturer's instructions (Vector Labs) and added to sections. Sections were washed in distilled water, dehydrated, and mounted using xylene mounting media (PROTOCOL).

Immunohistochemical staining for FPN was also performed on kidney sections from wild-type C57BL/6 mice. Kidneys were preserved by in vivo cardiac perfusion with PBS (pH 7.4) followed by periodate-lysine-2% paraformaldehyde (PLP), then cut transversely into several 2- to 4-mm-thick slices and immersed for approximately 24 hours at 4°C in the same fixative. Kidney samples from each animal were embedded in polyester wax (polyethylene glycol 400 distearate [Polysciences], 10% 1-hexadecanol), and 3-μm-thick sections were cut and mounted on triple chrome-, alum-, and gelatin-coated glass slides. Immunolocalization was accomplished using immunoperoxidase procedures described previously (57). Briefly, sections were dewaxed, rehydrated, and incubated in 3% H_2O_2 for 45 minutes to block endogenous peroxidase activity. Sections were blocked for 15 minutes with Serum-Free Protein Block (DakoCytomation), then incubated at 4°C overnight with primary antibody. The sections were washed in PBS and incubated for 30 minutes with polymer-linked, peroxidase-conjugated goat anti-rabbit IgG (MACH2, Biocare Medical), again washed with PBS, then exposed to diaminobenzidine (DAB) for 5 minutes. Sections were washed in distilled water, dehydrated with xylene, mounted, and observed by light microscopy.

For lotus lectin staining, embedding, sectioning, deparrafinization, rehydration, antigen retrieval, and peroxidase blocks were performed as above. Additionally, avidin/biotin blocking was performed using the avidin/biotin blocking kit (Vector Labs) per the manufacturer's instructions. Biotinylated lotus lectin diluted 1:400 in PBS was added for 1 hour. Sections were washed 3 times in PBS, then incubated in ABC ready-to-use reagent (Vector Labs) for 30 minutes and washed again. Chromogen substrate was diluted per the manufacturer's instructions (Vector Labs), and sections were washed, dehydrated, and mounted as above. Images were captured using a Leica DM IRB microscope (Leica Microsystems) and Image-Pro Plus software (Media Cybernetics).

Immunoelectron microscopy. Immunoelectron microscopy was performed as previously described, with minor modifications (58). Briefly, tissue samples were preserved by in vivo cardiac perfusion with PBS followed by 2% paraformaldehyde-lysine-periodate (PLP) fixative and stored overnight at 4°C. Samples were rinsed in PBS, treated with 0.1M NH_4Cl, and then dehydrated in a graded series of ethanols, embedded in Lowicryl K4M (Electron Microscopy Sciences), and polymerized under UV light for 24 hours at –20°C and for 64 hours at room temperature. Ultrathin (60–70 nm) sections of samples containing well-preserved proximal tubules were cut and mounted on formvar/carbon-coated nickel grids. FPN localization was detected using immunogold cytochemistry. Briefly, sections were exposed to 0.1M NH_4Cl and to 1% BSA to block nonspecific binding, treated with the anti-FPN antibody (Abcam; 1:25) overnight at 4°C, rinsed, treated with anti-rabbit secondary antibody conjugated to 0.8 nm colloidal gold (Aurion Ultrasmall Immunogold Conjugate, Electron Microscopy Sciences), washed, postfixed, washed, silver-enhanced (Aurion R-Gent SE-EM, Electron Microscopy Sciences), washed, and counterstained with uranyl acetate. A negative control section was exposed to incubation buffer in place of the primary antibody. Sections were observed and imaged using a Hitachi H-7600 transmission electron microscope (Hitachi High-Technologies America) equipped with a Macrofire monochrome progressive-scan CCD camera (Optronics) and AMT image capture software (version 600.335h; Advanced Microscopy Techniques).

Western blot analysis. Harvested cells or collected tissues were lysed in RIPA buffer (50 mmol/l Tris/HCl, 1% NP-40, 0.25% deoxycholic acid,

150 mmol/l NaCl, 1 mmol/l EGTA, 1 mmol/l sodium orthovanadate, and 1 mmol/l sodium fluoride) with protease inhibitor (Sigma-Aldrich) and quantified using BCA protein assay (Thermo Scientific). Total protein (10–15 μg for cells, 2 μl of urine, and 75 μg for tissues) was resolved on a 12% Tris-glycine sodium dodecyl sulfate polyacrylamide gel electrophoresis and transferred to a polyvinylidene fluoride membrane (Millipore). Membranes were blocked with 5% nonfat dry milk in PBST for 1 hour and then incubated with a rabbit anti-FtH antibody (Santa Cruz Biotechnology, 1:5,000), a rabbit anti-SCL40A1 (FPN) antibody (Alpha Diagnostic; 1:1,000), a rabbit anti-NRAMP2 (DMT-1) antibody (Santa Cruz Biotechnology, 1:1,000), a rabbit anti–HO-1 antibody (Enzo LifeSciences; 1:2,000), a rabbit anti–cleaved caspase-3 antibody (Cell Signaling; 1:2,000), or a goat anti-NGAL antibody (R&D Systems; 1:2,000) followed by a peroxidase-conjugated goat anti-rabbit or -mouse IgG antibody or donkey anti-goat IgG antibody (Jackson ImmunoResearch Laboratories; 1:10,000). Horseradish peroxidase activity was detected using an enhanced chemiluminescence detection system (GE Healthcare). The membrane was stripped and probed with anti-GAPDH antibody (Sigma-Aldrich; 1:5,000) to confirm loading and transfer. Densitometry analysis was performed, and results were normalized to GAPDH expression and expressed as fold change relative to controls. For FtL detection, samples were run on a native gel, transferred onto PVDF membrane, incubated with rabbit anti-FtL antibody (generated in house), followed by peroxidase-conjugated goat anti-rabbit antibody and detected using chemiluminescence, as described above. For transferrin and NGAL detection, 2 μl urine was resolved on a 12% Tris-glycine sodium dodecyl sulfate polyacrylamide gel electrophoresis, transferred onto PVDF membrane, blocked, incubated with goat anti-NGAL antibody (1:2,000) or mouse anti-transferrin antibody (Santa Cruz Biotechnology; 1:1,000) followed by a peroxidase-conjugated goat anti-mouse IgG antibody or donkey anti-goat IgG antibody (Jackson ImmunoResearch Laboratories; 1:10,000), and detected using chemiluminescence as described above.

ELISA. ELISA analyses for ferritin (Kamiya Biomedical Co.), NGAL (Bioporto Diagnostics), and transferrin and hemopexin (Alpha Diagnostic) were performed on serum or urine following the manufacturer's instructions. Urine creatinine was measured by LC-MS/MS (54). Data were expressed as micrograms per milliliter or were normalized to urine creatinine and expressed as micrograms per milligram creatinine.

Apoferritin and FtH treatment. Primary proximal tubular cells were isolated from wild-type mice as described previously (59) and immortalized by transfection with an SV40 plasmid. Cells were treated at various doses and times with apoferritin (Sigma-Aldrich). Cell lysates treated with 0, 0.5, and 1.0 mg/ml were collected in RIPA buffer containing protease inhibitor cocktail (Sigma-Aldrich) after 16 hours for Western blot analysis. Additionally, lysates treated with 1.0 mg/ml apoferritn were collected at time 0 and 8 hours in TRIzol for RNA analysis by real-time PCR as described above. Cells were treated with 0.5 mg/ml FtH or FtH-M (generated in house) for 16 hours and analyzed for FPN and FtH expression by Western blot as described above.

Polarization of proximal tubular cells and hepcidin treatment. Proximal tubular cells were plated on Transwell filters (Corning) with a pore size of 0.4 μm. Polarization was confirmed with immunocytochemistry for ZO-1 as previously described (60). Rat mAb R40.76 against ZO-1 was a gift from D.F. Balkovetz (University of Alabama at Birmingham, Birmingham, Alabama, USA). For hepcidin pretreatment, cells were treated with hepcidin (Peptides International; 400 nM) for 48 hours prior to iron uptake assay.

Iron uptake assay. Cells were washed with PBS and media devoid of transferrin, and serum was added to both apical and basal compartments. In the apical chamber, media was supplemented with 5 μM ^{55}Fe (PerkinElmer), and 200 μmol/l ascorbic acid was added to the media in order to ensure that iron was in the ferrous state. After 2 hours, media

from both the compartments was removed, and filters were washed at least 4 times with PBS. Cells were harvested in RIPA buffer, and radioactivity was measured in duplicates for each sample. The amount of iron in the cellular lysates was quantitated using a standard curve generated using known concentrations of ^{55}Fe. Protein content in each sample was measured, and data were expressed as picomoles of ^{55}Fe per milligram protein.

Statistics. Data are presented as mean ± SEM. Unpaired 2-tailed Student's *t* test was used for comparisons between 2 groups. For comparisons involving more than 2 groups, ANOVA and Newman-Keuls test were used. A *P* value less than 0.05 was considered significant. All experiments were performed at least 3 times.

Study approval. All procedures involving mice were performed in accordance with NIH guidelines for the use and care of live animals and were reviewed and approved by the IACUC of the University of Alabama at Birmingham.

Address correspondence to: Anupam Agarwal, Division of Nephrology, THT 647, University of Alabama at Birmingham, 1900 University Blvd., Birmingham, Alabama 35294, USA. Phone: 205.996.6670; Fax: 205.996.6650; E-mail: agarwal@uab.edu.

1. Xue JL, et al. Incidence and mortality of acute renal failure in Medicare beneficiaries, 1992 to 2001. *J Am Soc Nephrol.* 2006;17(4):1135–1142.
2. Shah SV, Walker PD. Evidence suggesting a role for hydroxyl radical in glycerol-induced acute renal failure. *Am J Physiol.* 1988;255(3 pt 2):F438–F443.
3. Paller MS. Hemoglobin- and myoglobin-induced acute renal failure in rats: role of iron in nephrotoxicity. *Am J Physiol.* 1988;255(3 pt 2):F539–F544.
4. Nath KA. Heme oxygenase-1: a provenance for cytoprotective pathways in the kidney and other tissues. *Kidney Int.* 2006;70(3):432–443.
5. Baliga R, Zhang Z, Baliga M, Ueda N, Shah SV. In vitro and in vivo evidence suggesting a role for iron in cisplatin-induced nephrotoxicity. *Kidney Int.* 1998;53(2):394–401.
6. Baliga R, Ueda N, Walker PD, Shah SV. Oxidant mechanisms in toxic acute renal failure. *Drug Metab Rev.* 1999;31(4):971–997.
7. Agarwal A, Nick HS. Renal response to tissue injury: lessons from heme oxygenase-1 gene ablation and expression. *J Am Soc Nephrol.* 2000;11(5):965–973.
8. Agarwal A, Balla J, Alam J, Croatt AJ, Nath KA. Induction of heme oxygenase in toxic renal injury: a protective role in cisplatin nephrotoxicity in the rat. *Kidney Int.* 1995;48(4):1298–1307.
9. Harrison PM, Arosio P. The ferritins: molecular properties, iron storage function and cellular regulation. *Biochim Biophys Acta.* 1996;1275(3):161–203.
10. Nath KA, et al. Induction of heme oxygenase is a rapid, protective response in rhabdomyolysis in the rat. *J Clin Invest.* 1992;90(1):267–270.
11. Thompson KJ, Fried MG, Ye Z, Boyer P, Connor JR. Regulation, mechanisms and proposed function of ferritin translocation to cell nuclei. *J Cell Sci.* 2002;115(pt 10):2165–2177.
12. Levi S, et al. A human mitochondrial ferritin encoded by an intronless gene. *J Biol Chem.* 2001;276(27):24437–24440.
13. Zarjou A, et al. Ferritin prevents calcification and osteoblastic differentiation of vascular smooth muscle cells. *J Am Soc Nephrol.* 2009;20(6):1254–1263.
14. Coffman LG, Parsonage D, D'Agostino R, Torti FM, Torti SV. Regulatory effects of ferritin on angiogenesis. *Proc Natl Acad Sci U S A.* 2009;106(2):570–575.
15. Zager RA. Combined mannitol and deferoxamine therapy for myohemoglobinuric renal injury and oxidant tubular stress. Mechanistic and therapeutic implications. *J Clin Invest.* 1992;90(3):711–719.
16. Baliga R, Zhang Z, Baliga M, Ueda N, Shah SV. Role of cytochrome P-450 as a source of catalytic iron in cisplatin-induced nephrotoxicity. *Kidney Int.* 1998; 54(5):1562–1569.
17. Ueda N, Guidet B, Shah SV. Gentamicin-induced mobilization of iron from renal cortical mitochon-
dria. *Am J Physiol.* 1993;265(3 pt 2):F435–F439.
18. Baliga R, Ueda N, Shah SV. Increase in bleomycin-detectable iron in ischaemia/reperfusion injury to rat kidneys. *Biochem J.* 1993;291(pt 3):901–905.
19. Paller MS, Hedlund BE. Role of iron in postischemic renal injury in the rat. *Kidney Int.* 1988; 34(4):474–480.
20. de Vries B, et al. Reduction of circulating redox-active iron by apotransferrin protects against renal ischemia-reperfusion injury. *Transplantation.* 2004; 77(5):669–675.
21. Mishra J, et al. Amelioration of ischemic acute renal injury by neutrophil gelatinase-associated lipocalin. *J Am Soc Nephrol.* 2004;15(12):3073–3082.
22. Hentze MW, Muckenthaler MU, Andrews NC. Balancing acts: molecular control of mammalian iron metabolism. *Cell.* 2004;117(3):285–297.
23. Andrews NC, Schmidt PJ. Iron homeostasis. *Annu Rev Physiol.* 2007;69:69–85.
24. Vanoaica L, Darshan D, Richman L, Schumann K, Kuhn LC. Intestinal ferritin H is required for an accurate control of iron absorption. *Cell Metab.* 2010; 12(3):273–282.
25. Pigeon C, et al. A new mouse liver-specific gene, encoding a protein homologous to human antimicrobial peptide hepcidin, is overexpressed during iron overload. *J Biol Chem.* 2001; 276(11):7811–7819.
26. Roetto A, et al. Mutant antimicrobial peptide hepcidin is associated with severe juvenile hemochromatosis. *Nat Genet.* 2003;33(1):21–22.
27. Darshan D, Vanoaica L, Richman L, Beermann F, Kuhn LC. Conditional deletion of ferritin H in mice induces loss of iron storage and liver damage. *Hepatology.* 2009;50(3):852–860.
28. Anderson GJ, Darshan D, Wilkins SJ, Frazer DM. Regulation of systemic iron homeostasis: how the body responds to changes in iron demand. *Biometals.* 2007;20(3–4):665–674.
29. Rankin EB, Tomaszewski JE, Haase VH. Renal cyst development in mice with conditional inactivation of the von Hippel-Lindau tumor suppressor. *Cancer Res.* 2006;66(5):2576–2583.
30. Patel YM, Yun JS, Liu J, McGrane MM, Hanson RW. An analysis of regulatory elements in the phosphoenolpyruvate carboxykinase (GTP) gene which are responsible for its tissue-specific expression and metabolic control in transgenic mice. *J Biol Chem.* 1994; 269(8):5619–5628.
31. Rankin EB, Higgins DF, Walisser JA, Johnson RS, Bradfield CA, Haase VH. Inactivation of the aryl-hydrocarbon receptor nuclear translocator (Arnt) suppresses von Hippel-Lindau disease-associated vascular tumors in mice. *Mol Cell Biol.* 2005; 25(8):3163–3172.
32. Ramey G, Deschemin JC, Durel B, Canonne-Hergaux F, Nicolas G, Vaulont S. Hepcidin targets ferroportin for degradation in hepatocytes. *Haematologica.* 2010; 95(3):501–504.
33. Baliga R, Zhang Z, Baliga M, Shah SV. Evidence for cytochrome P-450 as a source of catalytic iron in myoglobinuric acute renal failure. *Kidney Int.* 1996; 49(2):362–369.
34. Haase-Fielitz A, et al. Urine hepcidin has additive value in ruling out cardiopulmonary bypass-associated acute kidney injury: an observational cohort study. *Crit Care.* 2011;15(4):R186.
35. Prowle JR, et al. Greater increase in urinary hepcidin predicts protection from acute kidney injury after cardiopulmonary bypass. *Nephrol Dial Transplant.* 2012;27(2):595–602.
36. Ho J, et al. Urinary hepcidin-25 and risk of acute kidney injury following cardiopulmonary bypass. *Clin J Am Soc Nephrol.* 2011;6(10):2340–2346.
37. Mori K, et al. Endocytic delivery of lipocalin-siderophore-iron complex rescues the kidney from ischemia-reperfusion injury. *J Clin Invest.* 2005; 115(3):610–621.
38. Beaumont C, Delaby C. Recycling iron in normal and pathological states. *Semin Hematol.* 2009; 46(4):328–338.
39. Pantopoulos K, Porwal SK, Tartakoff A, Devireddy L. Mechanisms of mammalian iron homeostasis. *Biochemistry.* 2012;51(29):5705–5724.
40. Ward DM, Kaplan J. Ferroportin-mediated iron transport: expression and regulation. *Biochim Biophys Acta.* 2012;1823(9):1426–1433.
41. Beaumont C. Multiple regulatory mechanisms act in concert to control ferroportin expression and heme iron recycling by macrophages. *Haematologica.* 2010; 95(8):1233–1236.
42. Ganz T, Nemeth E. Hepcidin and iron homeostasis. *Biochim Biophys Acta.* 2012;1823(9):1434–1443.
43. Veuthey T, D'Anna MC, Roque ME. Role of the kidney in iron homeostasis: renal expression of Prohepcidin, Ferroportin, and DMT1 in anemic mice. *Am J Physiol Renal Physiol.* 2008;295(4):F1213–F1221.
44. Abouhamed M, et al. Divalent metal transporter 1 in the kidney proximal tubule is expressed in late endosomes/lysosomal membranes: implications for renal handling of protein-metal complexes. *Am J Physiol Renal Physiol.* 2006;290(6):F1525–F1533.
45. Kulaksiz H, et al. The iron-regulatory peptide hormone hepcidin: expression and cellular localization in the mammalian kidney. *J Endocrinol.* 2005; 184(2):361–370.
46. Smith CP, Thevenod F. Iron transport and the kidney. *Biochim Biophys Acta.* 2009;1790:724–730.
47. Zhang D, Meyron-Holtz E, Rouault TA. Renal iron metabolism: transferrin iron delivery and the role

of iron regulatory proteins. *J Am Soc Nephrol*. 2007; 18(2):401–406.

48. Yachie A, et al. Oxidative stress causes enhanced endothelial cell injury in human heme oxygenase-1 deficiency. *J Clin Invest*. 1999;103(1):129–135.

49. Poss KD, Tonegawa S. Heme oxygenase 1 is required for mammalian iron reutilization. *Proc Natl Acad Sci U S A*. 1997;94(20):10919–10924.

50. Kapturczak MH, et al. Heme oxygenase-1 modulates early inflammatory responses: evidence from the heme oxygenase-1-deficient mouse. *Am J Pathol*. 2004;165(3):1045–1053.

51. Ferguson CJ, Wareing M, Ward DT, Green R, Smith CP, Riccardi D. Cellular localization of divalent metal transporter DMT-1 in rat kidney. *Am J Physiol Renal Physiol*. 2001;280(5):F803–F814.

52. Cohen LA, et al. Serum ferritin is derived primarily from macrophages through a nonclassical secretory pathway. *Blood*. 2010;116(9):1574–1584.

53. Kim J, et al. In vivo regulation of the heme oxygenase-1 gene in humanized transgenic mice. *Kidney Int*. 2012; 82(3):278–291.

54. Takahashi N, Boysen G, Li F, Li Y, Swenberg JA. Tandem mass spectrometry measurements of creatinine in mouse plasma and urine for determining glomerular filtration rate. *Kidney Int*. 2007; 71(3):266–271.

55. Nath KA, Haggard JJ, Croatt AJ, Grande JP, Poss KD, Alam J. The indispensability of heme oxygenase-1 in protecting against acute heme protein-induced toxicity in vivo. *Am J Pathol*. 2000; 156(5):1527–1535.

56. Gutteridge JM, Rowley DA, Halliwell B. Superoxide-dependent formation of hydroxyl radicals in the presence of iron salts. Detection of 'free' iron in biological systems by using bleomycin-dependent degradation of DNA. *Biochem J*. 1981;199(1):263–265.

57. Verlander JW, et al. Dietary Cl(–) restriction upregulates pendrin expression within the apical plasma membrane of type B intercalated cells. *Am J Physiol Renal Physiol*. 2006;291(4):F833–839.

58. Wall SM, et al. Localization of pendrin in mouse kidney. *Am J Physiol Renal Physiol*. 2003;284:F229–F241.

59. Bolisetty S, et al. Heme oxygenase-1 inhibits renal tubular macroautophagy in acute kidney injury. *J Am Soc Nephrol*. 2010;21(10):1702–1712.

60. Balkovetz DF, Pollack AL, Mostov KE. Hepatocyte growth factor alters the polarity of Madin-Darby canine kidney cell monolayers. *J Biol Chem*. 1997; 272(6):3471–3477.